

# Topological effects of a vorticity filament on the coherent backscattering cone

Geoffroy J. Aubry<sup>1,\*</sup> and Philippe Roux<sup>2,†</sup>

<sup>1</sup>*Fachbereich Physik, Universität Konstanz, 78457 Konstanz, Germany*

<sup>2</sup>*Université Grenoble Alpes, CNRS, ISTERRE, 38000 Grenoble, France*

(Dated: September 1, 2022)

In this letter, we report on the effects of a vorticity filament on the coherent backscattering cone. Using ultrasonic waves in a strongly reverberating cavity, we show that through the number of loops of long-duration acoustic paths around a point-like vorticity filament located at the center of the cavity, the backscattering enhancement is destroyed, although it can also show periodic resurgences with increasing vorticity. The combination of the Aharonov-Bohm effect in acoustics and weak localization highlights topological phenomena in wave physics and tackles the relation between reciprocity and the coherent backscattering cone.

Coherent backscattering enhancement of waves by a random medium provides convincing evidence of interference effects despite disorder and multiple scattering. The coherent backscattering cone (CBC) manifests as a cusp in the angular distribution of the backscattered intensity [1]. This universal phenomenon has been observed experimentally at different spatial scales in optics [2], acoustics [3], and seismology [4], and with elastic waves [5] and cold atoms [6].

The CBC is considered to be a sign of weak localization of waves that propagate in a disordered medium. The weak localization originates from constructive interferences between multiple scattering paths and their reciprocal counterparts that follow the same sequence of scatterers in reverse order. Indeed, only reciprocity breaking in the propagation medium can alter the constructive interferences and destroy the enhancement [7]. Suppression of the CBC by Faraday rotation of light in a multiple scattering medium provided the first experimental evidence of the disappearance of weak localization [8]. Evidence of CBC destruction using acoustic waves in a rotational flow was also reported [9].

In this letter, we go one step beyond the CBC destruction by showing the potential rebirth of the cone for acoustic waves. Compared to the reciprocity-breaking phase shift induced by solid rotation, which depends on the statistical properties of conjugated paths, the topological anomaly created at the center of the cavity by a vorticity filament quantized wave transport properties: the *only* physical parameter that drives the CBC enhancement is the *integer number* of loops of the conjugated paths around this topological singularity.

The experimental setup is shown in the inset of Figure 1. A cylindrical metallic cavity (diameter, 15 cm; height, 10 cm) is filled with water. Two coplanar linear arrays  $T_1$  and  $T_2$  of  $N = 64$  ultrasonic transducers

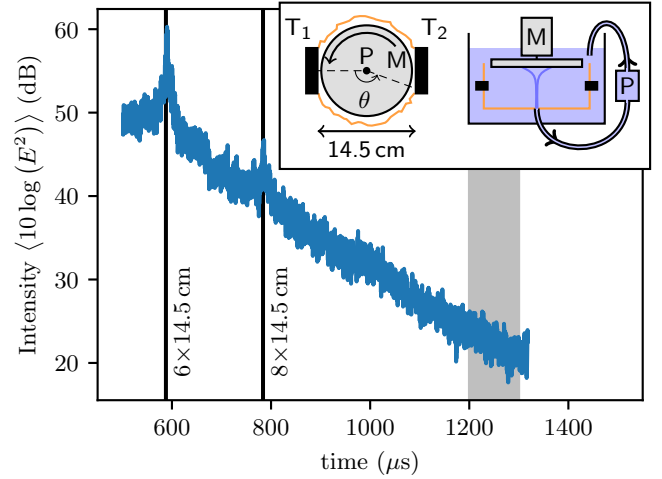


Figure 1. Intensity of the acoustic wave emitted and received by  $T_1$  as a function of time. Two specular reflections are visible. The black vertical lines correspond to the propagation times of the wave for the distances indicated. The gray domain corresponds to a typical time window over which the CBC is measured. Inset: The experimental setup.

centered at  $f = 6$  MHz are placed face to face at the half-height of the cavity, and are separated from each other by 14.5 cm. Each transducer of the array is  $L \simeq 10$  mm high and  $dx = 0.75$  mm  $\simeq 3\lambda$  wide, where  $\lambda$  is the ultrasonic wavelength. A motor (Fig. 1 inset, M) drives a circular plate (diameter, 14 cm) that is positioned at the top of the cylinder, and a pump (Fig. 1 inset, P) draws water through a hole (diameter, 8 mm) in the center of the bottom surface of the cylinder. In combination with the rotating plate, this creates a single and stable vorticity filament with core radius  $r_0 \sim \lambda$  [10]. Note that if the pump is turned off, the upper rotating plate creates solid rotation in the cylindrical cavity with a typical dimension  $R \gg \lambda$  [9, 11]. In the first step, an ultrasonic plane wave can be transmitted through the vorticity filament by array  $T_1$ , and the phase shift of the direct incident plane wave induced by the flow can be measured on array  $T_2$ . As  $dx \ll L$ , this makes the plane wave propagate as a

\* geoffroy.aubry@uni-konstanz.de; Now at: Department of Physics, University of Fribourg, 1700 Fribourg, Switzerland

† philippe.roux@univ-grenoble-alpes.fr

collimated beam that is perpendicular to the vortex axis, with a relatively small extension along the vortex direction. The experimental configuration is thus close to the two-dimensional (2D) situation classically investigated in theoretical papers.

In the literature, the use of transducer arrays has provided spatial and dynamical characterization of rotating flows of different sizes [10, 12]. When the vortex size is large compared to the ultrasound wavelength, the phase shift is easily interpreted using geometrical acoustics, and it yields a direct measurement of the vortex circulation, size, and position. On the other hand, a vorticity filament (i.e., where the core size is smaller or comparable to the ultrasonic wavelength) behaves as a point-like scatterer in two dimensions. Sound scattering by a single vorticity filament has been intensively studied following the publication of the Lighthill classical theory of aerodynamic sound [13–18]. Theoretical and analytical analyses have been carried out to account for both sound scattering by the vortex core and long-range refraction effects due to the vortex flow [19, 20].

In 2D calculations, the scattered pressure field  $\psi$  is analogous to the classical quantum mechanics problem of a beam of charged particles incident on a magnetic field tube, a problem known as the Aharonov-Bohm effect [21, 22]. This formal analogy with quantum mechanics was first introduced by Berry et al. [23], who studied experimentally the scattering of surface waves by a bathtub vortex [24]. The signature of the ultrasound scattering by a single vortex was experimentally observed by Roux et al. [10], who reported that the analytical calculations based on the quantum analogy also hold for acoustics.

In practice, the vorticity filament is located at the center of the cavity around  $x = 0$ . The phase shift due to the wave-vorticity interaction on the transmitted signal between  $T_1$  and  $T_2$  is shown in Figure 2 for each of the transducers of the array  $T_2$ . Roux et al. [10] showed that the phase jump and the phase oscillations are well described by the wave function predictions of the quantum Aharonov-Bohm effect [22]

$$\psi_\alpha(\rho, \theta) = \sum_{m=-\infty}^{\infty} \exp\left[-i\frac{\pi}{2}|m-\alpha|\right] J_{|m-\alpha|}(k\rho) e^{im\theta}, \quad (1)$$

where the origin of the polar coordinates  $(\rho, \theta)$  is the vorticity filament, the angle  $\theta$  is counted from the backscattering direction (see setup scheme in Fig. 1), and  $k = 2\pi/\lambda$  is the wave number. The acoustic parameter  $\alpha$  can be deduced from the quantum mechanics analogy  $\alpha = \Gamma/\lambda c$ ,  $c$  is the sound speed, and  $\Gamma$  is the flow circulation. The fitting of the curves is shown in Fig. 2, and the extracted  $\alpha$  are plotted as a function of the angular velocity of the upper circular plate in Figure 2b. For comparison, we measured the same quantity when the pump

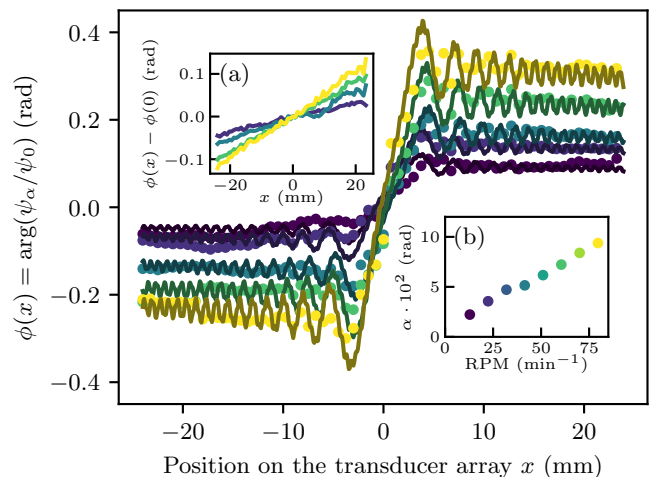


Figure 2. Phase shift for the transmitted signal between  $T_1$  and  $T_2$  induced by a vortex measured as a function of the rotation speed of the motor (color coded) at a given pump flow ( $0.06 \text{ L}\cdot\text{s}^{-1}$ ). The measurements are fitted to Eq. (1) to extract the vorticity parameter  $\alpha$  of the vortex (solid lines). Inset (a): The same quantity for solid rotation (i.e., pump turned off). Inset (b): The fitted vorticity parameter  $\alpha$  for the data plotted in the main Figure as a function of the rotation speed of the upper circular plate.

was turned off, i.e., for solid rotation of the water: linear dependency of the phase was measured along the array (see Fig. 2a), as expected by the radial velocity profile in the cavity for a solid rotation core larger than the array size.

To measure the coherent backscattering effects in the cavity, a plane wave is now emitted from array  $T_1$ , and the strongly reverberated and backscattered wavefield is recorded on the same array. To increase the random scattering properties of the cylindrical cavity in the 2D propagation plane, a stainless steel sheet with a root mean squared roughness  $\hat{h} = \sqrt{\langle h^2 \rangle} \simeq 0.55 \text{ mm}$  covers the inner boundary of the cylinder. The role of the rough metallic sheet that is glued to the cylinder wall is to scatter the incident ultrasonic wavefield and diminish the amplitude of the specular reflections, to obtain a quasi-2D cavity with rough boundaries. The intensity of a typical backscattered signal is shown in Fig. 1. To further avoid the contributions of specular reflections (i.e., the peaks in Fig. 1), we choose to record the signal over  $0.1 \text{ ms}$  after a lag time chosen between  $1.2 \text{ ms}$  and  $1.8 \text{ ms}$  (e.g., the gray region in Fig. 1 corresponds to such a typical time window). Following a method introduced by Aubry et al. [25], we then perform plane wave beamforming to recover the ultrasonic beams received in the directions around the incident plane-wave direction, with the power then calculated for the chosen time window. Compared to earlier point-like measurements of the CBC [9, 12] from an ultrasonic linear array, beamforming improves both the signal-to-noise ratio of strongly dispersed signals and

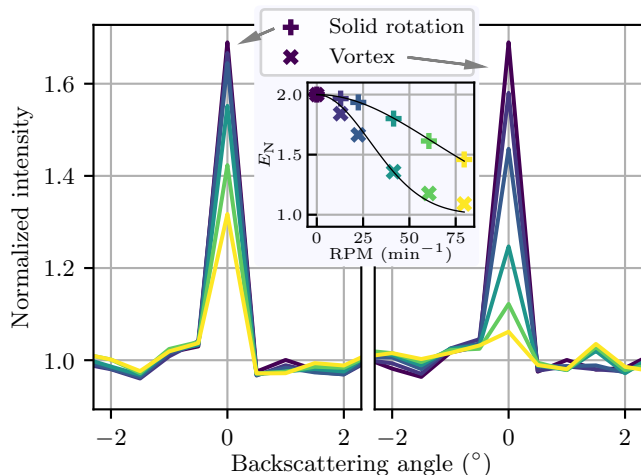


Figure 3. Coherent backscattering cones measured over 0.1 ms after 1.5 ms with solid rotation (left, no pump), and measured with a vorticity filament (right, pump imposing a flow of  $0.03 \text{ L}\cdot\text{s}^{-1}$ ). The same rotation speeds (color coded) were used without and with the pump. The darkest curves on both sides show the same measurements realized without any flow. Inset: Normalized enhancement factor  $E_N$  of the backscattering cones measured with solid rotation (+) and with a vorticity filament ( $\times$ ), as a function of the rotation speed of the upper plate.

the angular resolution of the intensity distributions, by a factor of 2 with the present array geometry.

To measure the CBC, there is the need to average over the disorder. In optics, this is achieved automatically in colloidal dispersions, and dry samples need to be moved to average over the speckles. Here, the cylindrical cavity has a fixed disorder that is given by the roughness of the metallic walls, and the positions of the transducers are fixed. Averaging over disorder can nevertheless be achieved by steering incident plane waves in different directions (typically every  $0.5^\circ$  from  $-10^\circ$  to  $10^\circ$ ), and by beamforming the received wavefield around each incident angle. The intensity averaged over the different incident directions  $I(\theta)$  is then normalized for its average value for  $|\theta| > 5^\circ$ . Such normalized intensities are shown in Figure 3. Note that the CBCs are measured here in a cavity with a typical width for the peak of  $\lambda/(Nd_x)$  (near field cone [5, 26]), which is close to the angular resolution of the ultrasonic array.

The darkest CBC in both panels of Figure 3 are measured without any flow in the cavity. In this case, the wave propagation obeys the reciprocity, and the enhancement factor (i.e., the value of the normalized intensity at  $0^\circ$ ) is expected to be 2. However, this is not the case here, where the enhancement factor is about 1.7, which is explained by the diffraction-limited  $3\lambda$  width of each transducer element. In the following, we define the normalized enhancement factor as  $E_N = \frac{E-1}{E_{\max}-1} + 1$ ,  $E_{\max} \simeq 1.7$ , which is the value of  $E$  without any flow.

The other CBCs of Figure 3 were measured with either solid rotation (left panel: upper plate turning, pump off) or a vorticity filament (right panel: upper plate turning, pump on). The colors encode the rotation speed of the upper plate, and correspond to the colors of the points in the inset. In both cases, the normalized enhancement factor decreases as a function of the rotation speed, as a signature of broken reciprocity [8]. However, in the inset of Figure 3, the normalized enhancement factor decreases more rapidly when there is a vorticity filament in the cavity ( $\times$ ), with respect to the case of solid rotation (+) for the same finite rotation speed.

The CBC shape depends on the path distributions inside the reverberating cavity. In the case of solid rotation, the radial velocity profile is  $\vec{v} = \Omega r \vec{u}_\theta$ , and the dephasing between the counter-propagating paths is

$$\Delta\varphi = \frac{4\pi}{\lambda c} \oint \vec{v} \cdot d\vec{\ell} = \frac{4\pi}{\lambda c} A\Omega, \quad (2)$$

where  $\Omega$  is the vorticity field and  $A$  is the area enclosed by the conjugated paths. The phase shift  $\Delta\varphi$  is then path dependent. Through calculation of the statistical properties of  $A$  for randomly scattered paths in a cavity, de Rosny et al. [12] provided an expression for the enhancement factor as a function of the solid rotation,

$$E(\Omega) \propto \exp\left[-\frac{\pi^3 R^3 t}{\lambda^2 c} \Omega^2\right], \quad (3)$$

where  $R$  is the radius of the solid rotation flow,  $t$  is the delay time at which the measurements were carried out, and  $\Omega$  is the vorticity of the flow. For the present geometry, Lehmkuhl et al. [11] experimentally measured the relation between  $\Omega$  and the rotation frequency  $f_0$  of the upper circular plate, as  $\Omega \simeq 0.3 \cdot f_0$ . Here, we fit the normalized enhancement factors  $E_N$  as a function of  $f_0$  by a Gaussian curve (Fig. 3 inset, solid lines). The only fit parameter —  $R = 4.0 \text{ cm}$  — has an acceptable value in the case of solid rotation in terms of boundary conditions associated with the cavity size and the flow measurements shown in Figure 2a. Nevertheless, the Gaussian fit is closer to the data points for the solid rotation (+) than for the vorticity filament case ( $\times$ ). This indicates that the different nature of both flows might change their phase shift characteristics qualitatively for long-duration wave propagation in the cavity. The rest of this article is devoted to the highlighting of the fundamental difference between the solid rotation and the vorticity filament case, from the CBC point of view.

For a vorticity filament, the radial velocity profile is  $\vec{v} = \frac{\Gamma}{2\pi r} \vec{u}_\theta$ , which leads to dephasing between counter-propagating paths (Eq. (2))

$$\Delta\varphi = \frac{4\pi}{\lambda c} n\Gamma = 4\pi\alpha \cdot n \quad (4)$$

The striking result here is that  $\Delta\varphi$  depends solely on the number of loops  $n$  around the vortex core, independent

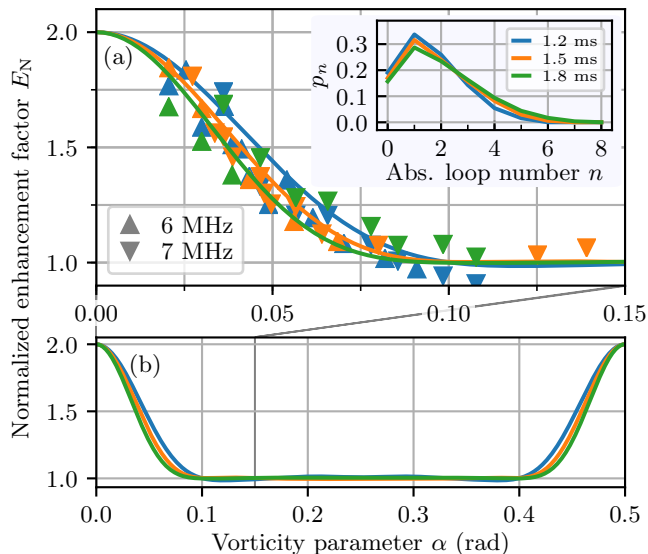


Figure 4. (a) Enhancement factor of the coherent backscattering cone as a function of the vorticity parameter  $\alpha$  for different frequencies of the wave (indicated by the symbols) and at different delay times. Each color corresponds to a delay time, and the corresponding theoretical curve is plotted in the same color. Inset: Plot of the absolute loop numbers calculated using the angular random walk model described in the text. (b) Predictions of the theory on a larger vorticity parameter range.

of the path trajectory, in agreement with the Aharonov-Bohm predictions. The phase shift acquired between two counter-propagating paths in the cavity in the presence of a vorticity filament (Eq. (4)) imposes the normalized intensity of the interference between these in the backscattering direction as  $1 + \cos \Delta\varphi$ . Defining  $p_n$  as the whole loop number distribution for closed paths in the cavity — which is independent of the presence of the vorticity filament, if the contribution of the field scattered by the vortex core is ignored — the enhancement factor  $E$  is then expected to be

$$E(\alpha) = \sum_{n \in \mathbb{N}} p_n [1 + \cos(4\pi n \alpha)]. \quad (5)$$

Figure 4(a) shows the values of the normalized enhancement factors  $E_N$  as a function of  $\alpha$  for different experimental conditions. Note that  $\alpha$  results from the combination of the rotation speed of the upper plate, the flow imposed by the pump, and the frequency of the acoustic wave.

To compute the values of  $E$  predicted by Eq. (5), the loop number distribution  $p_n$  around the vortex in the cavity needs to be defined. This distribution is numerically obtained using a random walk model that describes the propagation of acoustic waves in the circular 2D cavity. In the model, all of the paths start from  $T_1$ , and are emitted in a direction following a normal law centered in

the forward direction. The wave then propagates freely in the medium, and a scattering event happens each time the wave hits the circular wall of the 2D cavity. If the incident wave arrives at an angle  $\theta_i$  with respect to the normal of the cavity, it is then scattered in a direction  $\theta_s$ , according to the Kirchhoff and perturbation approximation for rough surface scattering [27]<sup>1</sup>. The random walk was continued until the path has the appropriate length that corresponds to the time window over which the CBC is measured, and we only keep the paths that end on array  $T_1$ . For these paths, the loop number is monitored around the vortex. A total of  $5 \cdot 10^4$  paths were simulated, and the resulting curve  $p_n$  of the absolute loop number  $n$  around the vortex is plotted as a function of the path length in Figure 4(a), inset. The higher the specular reflection at each scattering event, the higher the average loop number, and the faster the decrease for  $E(\alpha)$ .

Using the aforementioned  $p_n$ , we plot Eq. (5) in Fig. 4(a). Within the experimental error, there is a good agreement between the data and the theory. The model predicts that  $E(\alpha)$  is 0.5-periodic for any distribution of  $p_n$  (see Fig. 4(b)). In particular, this means that  $E(0.5) = 2$ , which is a major difference compared to solid rotation, where  $E$  strictly decreases to 1 for increasing motor frequency [12], and compared to the effects of Faraday rotation in optics [8], where  $E$  also irremediably decreases to 1 when the external magnetic field is increased.

However, can the ‘rebirth’ of the CBC be obtained with realistic experimental configurations? To answer this question, we assume a vortex core size  $r_0 \sim \lambda$  and a maximum flow velocity  $U_{\max}$ , which leads to  $\Gamma = 2\pi r_0 U_{\max}$ , and thus  $\alpha = 2\pi \frac{r_0}{\lambda} \frac{U_{\max}}{c} \sim 2\pi \text{Ma}$ , where  $\text{Ma} = U_{\max}/c$  is the flow Mach number. Values of the vorticity parameter  $\alpha = 0.5$  then induce  $\text{Ma} \sim 0.1$ , which is impossible to achieve in water because of the appearance of cavitation bubbles in the vortex core, which slow down the flow velocity. However,  $\text{Ma} \sim 0.1$  might be reachable with one single vorticity filament in a medium with lower sound velocities, such as air [28] or second sound in superfluid helium [29]. Finally, the rebirth of the CBC would pave the way to a striking manifestation of wave-vorticity topological interactions under strongly reciprocity breaking conditions.

The authors thank Georg Maret, and GJA acknowledges support from the Zukunftscolleg (Universität Konstanz) for a Mentorship grant. The authors wish to thank Frédéric Faure, Julien de Rosny, Bart van Tiggelen and Arnaud Tourin for fruitful discussions.

<sup>1</sup> The rough surface is described by the root-mean-square roughness  $\hat{h} \simeq 2\lambda$  and surface correlation length  $l = 2 \text{ mm} \gg \lambda$ .

- 
- [1] E. Akkermans, P. E. Wolf, and R. Maynard, *Phys. Rev. Lett.* **56**, 1471 (1986).
- [2] P.-E. Wolf and G. Maret, *Phys. Rev. Lett.* **55**, 2696 (1985); M. P. V. Albada and A. Lagendijk, *Phys. Rev. Lett.* **55**, 2692 (1985).
- [3] G. Bayer and T. Niederdränk, *Phys. Rev. Lett.* **70**, 3884 (1993).
- [4] E. Larose, L. Margerin, B. A. van Tiggelen, and M. Campillo, *Phys. Rev. Lett.* **93**, 048501 (2004).
- [5] J. de Rosny, A. Tourin, and M. Fink, *Phys. Rev. Lett.* **84**, 1693 (2000).
- [6] F. Jendrzejewski, K. Müller, J. Richard, A. Date, T. Plisson, P. Bouyer, A. Aspect, and V. Josse, *Phys. Rev. Lett.* **109**, 195302 (2012).
- [7] A. A. Golubentsev, *Sov. Phys. JETP* **59**, 26 (1984), original version in *Zhurnal Eksperimentalnoi I Teoreticheskoi Fiziki* 86 (1), pp.47-59 (1984).
- [8] F. A. Erbacher, R. Lenke, and G. Maret, *EPL (Europhysics Letters)* **21**, 551 (1993); L. Schertel, G. J. Aubry, C. M. Aegerter, and G. Maret, *The European Physical Journal Special Topics* **226**, 1409 (2017).
- [9] A. Tourin, A. Derode, P. Roux, B. A. van Tiggelen, and M. Fink, *Phys. Rev. Lett.* **79**, 3637 (1997).
- [10] P. Roux, J. de Rosny, M. Tanter, and M. Fink, *Phys. Rev. Lett.* **79**, 3170 (1997).
- [11] G. Lehmkuhl and J. Hudson, *Chemical Engineering Science* **26**, 1601 (1971).
- [12] J. de Rosny, A. Tourin, A. Derode, P. Roux, and M. Fink, *Phys. Rev. Lett.* **95**, 074301 (2005).
- [13] M. Lighthill, *Proceedings of the Royal Society of London A: Mathematical, Physical and Engineering Sciences* **211**, 564 (1952).
- [14] A. Fetter, *Phys. Rev.* **136**, A1488 (1964).
- [15] S. O'Shea, *Journal of Sound and Vibration* **43**, 109 (1975).
- [16] A. L. Fabrikant, *Akusticheski Zhurnal* **28**, 694 (1982), translated in *Soviet Physics Acoustics* **28**, 410 (1982).
- [17] P. V. Sakov, *Akusticheski Zhurnal* **39**, 537 (1993), translated in *Acoustical Physics* **39**, 280 (1993).
- [18] S. Manneville, P. Roux, M. Tanter, A. Maurel, M. Fink, F. Bottausci, and P. Petitjeans, *Phys. Rev. E* **63**, 036607 (2001).
- [19] J. Reinschke, W. Möhring, and F. Obermeier, *Journal of Fluid Mechanics* **333**, 273–299 (1997).
- [20] R. Ford and S. G. Llewellyn Smith, *Journal of Fluid Mechanics* **386**, 305–328 (1999).
- [21] Y. Aharonov and D. Bohm, *Phys. Rev.* **115**, 485 (1959).
- [22] S. Olariu and I. I. Popescu, *Rev. Mod. Phys.* **57**, 339 (1985).
- [23] M. V. Berry, R. G. Chambers, M. D. Large, C. Upstill, and J. C. Walmsley, *European Journal of Physics* **1**, 154 (1980).
- [24] F. Vivanco, F. Melo, C. Coste, and F. Lund, *Phys. Rev. Lett.* **83**, 1966 (1999).
- [25] A. Aubry, A. Derode, P. Roux, and A. Tourin, *The Journal of the Acoustical Society of America* **121**, 70 (2007).
- [26] R. L. Weaver and J. Burkhardt, *The Journal of the Acoustical Society of America* **96**, 3186 (1994).
- [27] E. I. Thorsos, *The Journal of the Acoustical Society of America* **83**, 78 (1988); A. Ishimaru, in *Wave Propagation and Scattering in Random Media*, edited by A. Ishimaru (Academic Press, 1978) pp. 463 – 492.
- [28] J.-F. Pinton and G. Brillant, *Theoretical and Computational Fluid Dynamics* **18**, 413 (2005).
- [29] R. Donnelly, *Physics Today* **62**, 34 (2009).